Distinct ROPGEFs successively drive polarization and outgrowth of root hairs

AUTHORS:

Philipp Denninger[1,6], Anna Reichelt[1,6], Vanessa A. F. Schmidt[1], Dietmar G. Mehlhorn[3], Lisa Y. Asseck[3], Claire E. Stanley[4,5], Nana F. Keinath[1], Jan-Felix Evers[1], Christopher Grefen[3] and Guido Grossmann[1,2,*]

AFFILIATIONS:

[1]Centre for Organismal Studies (COS), Heidelberg University, Im Neuenheimer Feld 230, 69120 Heidelberg, Germany

[2]Excellence Cluster CellNetworks, Heidelberg University, Im Neuenheimer Feld 267, 69120 Heidelberg, Germany

[3]Center for Plant Molecular Biology, Developmental Genetics, University of Tübingen, Auf der Morgenstelle 32, 72076 Tübingen, Germany

[4]Institute for Chemical and Bioengineering, ETH Zürich, Vladimir-Prelog-Weg 1, 8093 Zürich, Switzerland

[5]Agroecology and Environment Research Division, Agroscope, Reckenholzstrasse 191, 8046 Zürich, Switzerland

[6]These authors contributed equally.

*Corresponding author:
Guido Grossmann
Centre for Organismal Studies
Im Neuenheimer Feld 230
69120 Heidelberg
Germany
email: guido.grossmann@cos.uni-heidelberg.de
ORCID ID: 0000-0001-7529-9244

SUMMARY

Root hairs are tubular protrusions of the root epidermis that significantly enlarge the exploitable soil volume in the rhizosphere. Trichoblasts, the cell type responsible for root hair formation, switch from cell elongation to tip growth through polarization of the growth machinery to a pre-defined root hair initiation domain (RHID) at the plasma membrane. The emergence of this polar domain resembles the establishment of cell polarity in other eukaryotic systems [1-3]. Rho-type GTPases of plants (ROPs) are among the first molecular determinants of the RHID [4,5] and later play a central role in polar growth [6]. Numerous studies have elucidated mechanisms that position the RHID in the cell [7-9] or regulate ROP activity [10-18]. The molecular players that target ROPs to the RHID and initiate outgrowth, however, have not been identified. We dissected the timing of the growth machinery assembly in polarizing hair cells and found that positioning of molecular players and outgrowth are temporally separate processes that are each controlled by specific ROP guanine nucleotide exchange factor (GEFs). A functional analysis of trichoblast-specific GEFs revealed GEF3 to be required for normal ROP polarization and thus efficient root hair emergence, while GEF4 predominantly regulates subsequent tip growth. Ectopic expression of GEF3 induced the formation of spatially confined, ROP-recruiting domains in other cell types, demonstrating the role of GEF3 to serve as a membrane landmark during cell polarization. Our findings suggest that morphogenetic programs in plants employ distinct regulatory modules for the alignment and activation of the cellular growth machinery.

RESULTS AND DISCUSSION

Temporal analysis of hair cell polarization reveals phased deployment of the tip-growth machinery

To dissect the process of breaking cellular symmetry and initiating polar growth in plants, we analyzed the gradual assembly of the tip growth machinery in trichoblasts using specific markers for cytoskeletal rearrangement, plasma membrane specialization, cell wall modification, vesicle trafficking, and Rho-GTPase signaling. Using stable transgenic *Arabidopsis* lines expressing fluorescently labeled versions of these protein markers, we determined the timing of their polarization at the RHID during trichoblast differentiation. As the *Arabidopsis* root represents a time-axis of development from stem cells to mature cells, we numbered the developmental stages (-7 to +3) within a cell file, with the first cell to exhibit a detectable bulge as stage +1 (**Figure 1A**). We used the integral plasma membrane marker GFP-LTI6B [19] as a reference and calculated the polarity index of fluorescently labeled marker proteins to quantify protein accumulation at the RHID (**Figure 1B**). Our survey unveiled a two-phase assembly of the tip growth machinery: an initiation phase, during which the RHID is positioned and predefined, followed by the tip growth phase. Consistent with previous reports [4,5], mCitrine-labeled (mCit) GTPase ROP2 associated with the RHID during the early initiation phase (stage -4), well before any detectable cell bulging (**Figure 1B, C, Supplemental Figure S1**). The timing of mCit-ROP2 polarization appeared to be largely independent from promoter activity, as analysis of an estradiol-inducible reporter construct for mCit-ROP2 resulted in a similar timing of RHID association, albeit with higher cytosolic signal (**Figure 1C, Supplemental Figure S1**). Closely related GTPases ROP4 and ROP6 exhibited a similar timing as ROP2, when inducibly expressed (**Figure 1C, Supplemental Figure S1**), which indicates that ROP GTPases are prepositioned well before growth is activated. The only tested ROP-effectors that were found to polarize after ROPs but still during the initiation phase, were the PHOSPHATIDYLINOSITOL-4-PHOSPHATE 5-KINASE 3 (PIP5K3) [20], and the NADPH oxidase ROOT HAIR DEFECTIVE 2 (RHD2) [21,22]. PIP5K3 and RHD2 have both been shown to be involved in ROP-dependent root hair growth regulation by modulating vesicle traffic to the plasma membrane and cell wall rigidity, respectively.

The second phase of root hair emergence was characterized by the polarization of known ROP effectors such as (ARPC2), a subunit of the actin polymerizing ARP2/3 complex [23], and the markers for vesicle transport and secretion SYP123 and SEC3A [24-26] (**Figure 1C, Supplemental Figure S1**). The onset of bulge formation was further characterized by local elevation of cytosolic Ca^{2+} as reported by the sensor RGECO-1 [27,28], as well as the formation of $PI(4,5)P_2$ at the emerging apex as indicated by the reporter P15Y [29]. The receptor-like kinase FERONIA, which activates ROPs during root hair tip growth [30], accumulated after bulging in stage +2 (**Figure 1C, Supplemental Figure S1**). The temporal separation of ROP positioning and growth activation led us to the conclusion that ROP regulation must also be temporally controlled.

Therefore, we hypothesized that upstream regulators of ROP GTPases exist, that are in charge of phase-specific ROP recruitment and control their activation.

ROPGEFs exhibit specific spatiotemporal patterns of expression and subcellular localization

ROPs have been extensively studied during cell elongation [31], stomata regulation [32], pavement cell development [33,34], and in regulation of the two tip-growing plant cell types, pollen tubes [35] and root hairs [4,5]. As molecular “switches”, the activity-state of GTPases depends on regulators that “toggle” the switch between active or inactive [36,37]. GTPase-activating proteins (GAPs) facilitate the catalytic cleavage of a bound GTP to GDP, rendering the GTPase inactive. Guanyl-nucleotide exchange factors (GEFs) replace the bound GDP for a GTP, thereby switching the GTPase into an active state and enabling the interaction with downstream effectors [37,38].

To identify candidate ROP regulators that play potential roles in root hair initiation and growth regulation we mined cell-type-specific gene expression data [39-41] and compared expression profiles of ROPGEFs of the PRONE family [42] and SPK1, the only DOCK family GEF [43], in root trichoblasts and atrichoblasts. Among these ROPGEFs (hereafter abbreviated as GEFs), the expression of GEF3 and GEF4 showed the strongest root hair-specificity, followed by GEF12, GEF11, GEF14, and GEF10 in descending order (**Supplemental Figure S2**). Other GEFs, including SPK1, did not exhibit stronger expression in hair cells and were therefore excluded from further analysis. To determine in which stage of hair cell maturation the candidate GEFs play their roles, we created translational fusions to mCitrine under the control of the respective native promoters and analyzed their expression pattern in growing roots. We observed a diverse distribution of expression patterns among the remaining GEFs, with a surprisingly unique pattern for each gene (**Figure 2A**). We further analyzed the timing of polarization at the RHID for each mCit-labeled GEF and compared it to the timing of mCit-ROP2. We found that mCit-GEF3 and mCit-GEF14 reached significant polarization consistently one cell stage earlier than mCit-ROP2 (**Figure 2B**). A major difference between both expression patterns was that GEF14 expression lasted from the meristematic zone (MZ) to the elongation zone (EZ), whereas GEF3 expression was first observed in the root transition zone (TZ, in-between MZ and EZ) and lasted beyond hair emergence (**Figure 2A**). The beginning of gene expression of GEF4 and GEF12 was detected first in EZ and the polarization of both proteins at the RHID coincided with the onset of bulge formation (**Figure 2A, B**). This specific behavior of highly related genes indicates that they take over specialized functions during defined time windows in differentiating cells.

In addition to the specific expression pattern of GEF3, its localization stood out in comparison to all other GEFs, as mCit-GEF3 appeared highly polarized at the cell periphery of the RHID (**Figure 2A, C**). While other GEFs, like mCit-GEF4, exhibited a lower degree of polarization and association with the plasma membrane (**Figure 2A, D**). mCit-GEF3 appeared highly concentrated in a circular polar domain with a diameter of 9.6 µm (± 2.5 µm), being barely detectable outside this domain (polarity index at cell "+1": 14.4 ± 2.2) (**Figure 2C, Supplemental Figure S3**). We tested

whether the timing of GEF polarization was dependent on the timing of gene expression and analyzed the polarity indices of mCit-GEF3 and mCit-GEF4 under the control of estradiol-inducible promoters. In both cases, the earlier gene expression did not result in an earlier RHID polarization of the protein (**Supplemental Figure S1**), but rather delayed the time point of significant polarization, likely due to higher cytosolic levels that affected the polarity index calculation. Its independence from gene expression indicates that the timing of polarization is an intrinsic feature that may be controlled by further partners of unknown identity.

To determine the functional role of the investigated GEFs we analyzed T-DNA insertion lines for phenotypes in root hair initiation and development. Root hair density was used as a measure for the general ability to develop root hairs, distance of the first bulge from the root tip was used to analyze delays in the timing of root hair initiation and root hair length was used as measure for regulation of tip growth. Only in *gef3* mutant alleles, root hair density was reduced and root hair initiation was delayed, (**Figure 2E - G, Supplemental Figure S4**), while hair length seemed only slightly affected (**Figure 2H**). In *gef3-1*, which lacks almost all full length transcript, the observed phenotypes could be rescued with a GEF3::mCit-GEF3 construct (**Supplemental Figure S4**), further verifying that loss of GEF3 function causes the phenotypes and confirming the functionality of the fusion construct. Furthermore, other mutant alleles of *gef3* showed a similar delay in root hair initiation (**Supplemental Figure S4**). All other *gef* mutants, including *gef4-2*, exhibited no negative effects on bulge distance or root hair density (**Figure 2E - G**), but *gef4-2* lines did show a reduced hair length (**Figure 2H**). This indicates distinct roles for GEF3 and GEF4, where GEF3 is responsible for root hair initiation and bulging, while GEF4 is regulating root hair tip growth.

GEF3 is required for efficient root hair emergence and polar recruitment of ROP2

We have shown that GEF3 accumulated very specifically at the RHID, preceded ROP2 accumulation, and was required for proper root hair development. Therefore, GEF3 was selected as a promising potential regulator of ROP dependent root hair initiation.

To determine the temporal relationship of GEF3 and ROP2 recruitment to the RHID in detail, we observed the localization of both proteins at higher resolution over time. We employed a new microfluidic device, termed RootChip-8S, for long-term imaging of growing *Arabidopsis* roots. The RootChip-8S, is an adapted version of previously published RootChip designs [44-46] and consists of eight separate observation chambers that can be individually perfused to provide stable growth conditions and restrict root movement in Z to prevent focal drift (**Supplemental Figure S5**). The first detectable signal of GEF3::mCit-GEF3 was observed in the transition zone of the root, shortly after the last cell division (**Figure 2 A and 3 A**). Time-lapse imaging showed early targeting of mCit-GEF3 to the rootward cell pole (**Figure 3 A**). As the protein gradually enriched at the RHID over approximately 30 min, its localization at the rootward cell pole vanished (**Figure 3 A, B**). The GEF3 domain eventually stabilized at a consistent diameter of 9.6 µm (± 2.5 µm; *n*=17; FWHM), with its center 9.0 µm (± 2.2 µm) from the rootward cell pole (**Figure 3 B, Supplemental Figure S3**). To validate the earlier RHID accumulation of GEF3 compared to ROP2 through simultaneous

visualization in the same cells, we imaged their localization in growing roots co-expressing fluorescently labeled versions of both proteins and found that mCit-GEF3 accumulated at the RHID one stage earlier than mTurquoise2-ROP2 (mTq2-ROP2) (**Figure 3 C**).

To test if GEF3 directly influences ROP2 recruitment to the RHID, we expressed mCit-ROP2 in the *gef3-1* T-DNA insertion mutant. Strikingly, we did not observe any significant polarization of mCit-ROP2 in the *gef3-1* mutant (**Figure 3 D, E**). Some cells in *gef3-1* were still able to produce bulges, but these bulges lacked polar ROP2 accumulation (**Figure 3 D, E**). Interestingly, the general membrane association of mCit-ROP2 was unaffected, as the localization appeared similar to that in other cell types. This shows that GEF3 function is required for ROP2 recruitment specifically to the RHID.

If the lack of ROP activity is responsible for the phenotypes observed in *gef3-1* mutants, loss of function mutants of ROPs should have similar phenotypes. We combined 2 previously described T-DNA lines for ROP2 and ROP4 [33,47], and analyzed the single mutants and the double mutant line for phenotypes in root hair initiation. For both traits, root hair density and distance of the first bulge to the root tip, the double mutant *rop2-1/rop4-1* showed a clear phenotype, while the single mutant lines showed no significant effects (**Figure 3 F - H**). Thus, lack of GEF3 or ROP2/ROP4 results in similar phenotypes, indicating a functional link between these proteins. In contrast to the loss of ROP2 polarity in *gef3-1* mutants, mCit-GEF3 polarity is still observed in *rop2-1/rop4-1* mutants (**Figure 3 I, K**). mCit-GEF3 polarity was unaffected in the early elongation zone (**Figure 3 I, K; Stage I**), but was slightly reduced in later stages (**Figure 3 I, K; Stage II & III**) compared to mCit-GEF3 polarity in Col-0 background (**Supplemental Figure S1**). This indicates that initial GEF3 polarization is largely ROP independent, while in later stages of root hair development GEF3 polarity is positively affected by ROPs. The question remained how GEF3 fulfills its function as a factor directing polarization of ROP2. To test if GEF3 was capable of recruiting ROP2 through physical interaction, we used a ratiometric bimolecular fluorescence complementation (rBiFC) assay with GEF3-cYFP with either an nYFP-carrying ROP2 (wild-type), a constitutively active CA-ROP2 (G14V), a dominant-negative DN-ROP2 (D120A), or a truncated *rop2*ΔN (Δ1-79) that lacks its interaction domain (**Supplemental Figure S6**) [5,48], co-expressed transiently in *Nicotiana benthamiana* leaf epidermis cells [49]. All GEF3-cYFP/nYFP-ROP2 combinations, except for *rop2*ΔN, resulted in detectable YFP fluorescence (**Figure 3 L, M, Supplemental Figure S6**). This finding was corroborated by a split-ubiquitin assay in yeast [50], testing the same putative interactor combinations. Except for *rop2*ΔN, all forms of ROP2 yielded yeast growth, indicating physical interaction with GEF3 (**Supplemental Figure S6**). This shows that GEF3 physically interacts with the active and inactive form of ROP2 via its interaction domain. Consistently, mCit-*rop2*ΔN expressed in *Arabidopsis* trichoblasts did not assume polar localization at the RHID (stage +1, **Figure 3 N, O**), demonstrating that the interaction domain of ROP2 is required for its RHID recruitment.

These results show that GEF3 is necessary for ROP polarization by recruiting ROP2 to the RHID via direct physical interaction. Furthermore, ROP activity is not essential for GEF3 polarization, but enhances GEF3 polarity.

GEF3 defines the RHID and guides ROP polarization

To investigate whether GEF3 is not only necessary but also sufficient for ROP2 polarization, we studied transgenic lines, inducibly overexpressing mCit-GEF3 (mCit-GEF3ox) in Col-0 or in ROP2::mTq2-ROP2 background. Upon overexpression of mCit-GEF3 we observed that additional patch-like GEF3 domains formed in trichoblasts and, surprisingly, also in atrichoblasts (**Figure 4 A**). Interestingly, in overexpression lines, we frequently observed mCit-GEF3 accumulation at the shootward sides of cells in the meristem or the early elongation zone (**Figure 4 A**). The final position of the primary RHID was not altered compared to Col-0 (**Supplemental Figure S7**). All observed normal and ectopic mCit-GEF3 accumulations resulted in the simultaneous recruitment of mTq2-ROP2 (**Figure 4 A**).

We took advantage of the ubiquitous overexpression of mCit-GEF3 and determined its localization in cells outside the root. In epidermal cells of the hypocotyl, we observed multiple occurrences of ectopic GEF3 accumulation into domains that strikingly resembled those of RHIDs in trichoblasts (**Figure 4 B**). Consistently, these ectopic mCit-GEF3 domains also lead to recruitment of mTq2-ROP, which never occurred in hypocotyl cells under control conditions (**Figure 4 B**). Except for trichoblasts, mCit-GEF3ox did not lead to bulge formation in other cells, indicating that ROP polarization alone was not sufficient to trigger outgrowth and further trichoblast-specific factors are required.

Since the analysis of gene expression, protein localization and loss-of-function phenotypes all suggested a differential timing of GEF3 and GEF4 function, we hypothesized that gain-of-function phenotypes should also reflect their specific roles in root hair initiation and growth. We therefore compared the phenotypic effects of mCit-GEF3ox to mCit-GEF4ox, which is known to induce root hair branching in trichoblasts [51]. In mCit-GEF4ox lines, bulges with branched tips, which failed to form long tube-like hairs, occurred in 30.5% of the observed cells (**Figure 4 C, D**). mCit-GEF3ox roots also displayed root hairs with branched tips in 20.6% of all trichoblasts, resembling mCit-GEF4 overexpression (**Figure 4 C, D**). However, mCit-GEF3ox further led to the formation of additional bulges, with 5.5% of trichoblasts showing multiple unbranched bulges and 21.4% of the cells showing multiple branched bulges within one cell (**Figure 4 C, D**). This phenotype bears striking similarities to *scn1* mutants that lack a ROP-inhibiting RhoGDI [11], which further points towards a gain of ROP activity in mCit-GEF3ox roots at an early stage during RHID positioning. We observed mCit-GEF3 accumulations in tips of branched root hairs and mTq2-ROP2 was generally present in the same locations (**Figure 4 E**), thus confirming that mCit-GEF3ox was also responsible for the formation of additional polar domains in branching hairs. These differential effects of GEF3 and GEF4 overexpression resemble the differential timing of their polar localization and further support the hypothesis that both proteins serve specific functions during different

phases of root hair development, with GEF3 being decisive for the early formation of the RHID and ROP2 recruitment, and GEF4 being involved in downstream activation of ROP2 to trigger growth.

GEFs serve as positional cues during cell polarization

To our knowledge, GEF3 is not only the first ROPGEF member reported to precede ROP polarization during tip growth initiation, but it is also the first example for a plant protein that, when overexpressed, is capable of inducing the ectopic formation of polar, ROP-recruiting domains. Our finding, that GEF3 acts upstream of ROP2, challenges the idea that ROPs are self-organizing key initiators of cell polarization [52]. Our results suggest a GEF3-mediated recruitment and temporally controlled ROP activation by differentially timed GEFs at this predefined location. Therefore, the previously modeled self-assembly mechanism of ROP2 at the RHID may not be the only driving force for polarization.

Evidence for a GTPase-positioning function of GEFs can also be found in other organisms. Recent work shows that during cellularization in Drosophila embryos, the GEF Dizzy and the heteromeric GEF complex ELMO-Sponge are required for polarization of the GTPase Rap1 [38,53]. It remains, however, challenging to establish the molecular sequence of GEF and GTPase functions in the context of a developing embryo. In budding yeast, Cdc42 is activated by its GEF Cdc24 during both budding and shmoo formation [54-56]. To initiate budding in yeast, the GEF Bud5 is recruited to the edge of the previous cell-division site by the landmark Axl2 [57]. Stabilized by scaffold proteins, Bud5 and the GEF Cdc24 then locally activate the GTPases Rsr4 and Cdc42 [58-63].

Using a GEF-scaffold complex as landmark for the targeted deployment of the growth machinery may therefore represent a common design principle among eukaryotic cells to prevent spontaneous and random polarization and, instead, drive growth in a directed manner. Yet, the fact that ROPGEFs share no conserved features with animal or fungal GEFs [42], indicates that the problem of robust cell morphogenesis has been solved several times during evolution to account for specific differences in cellular growth mechanisms, organ development and lifestyle.

MATERIALS AND METHODS

Plant material

Arabidopsis thaliana ecotype Col-0 was used as wildtype in this study. The mutant lines *rop2-1* (SALK_055328C), *gef3-1* (SALK_079879C), *gef3-2* (SALK_079885), *gef3-3* (SAIL_294_A09), *gef3-4* (SALK_021751) *gef3-5* (SALK_046978C) *gef4-2* (SALK_107520) were obtained from NASC (Nottingham Arabidopsis Stock Centre http://arabidopsis.info/). The *rop4-1* mutant [34] was kindly provided by Markus Grebe (Potsdam). Double mutants were made by crossing and selection for double homozygous plants by PCR (Primers used for genotyping, see Table S3). The GFP-SYP123 and GFP-SYP132 lines [24] were kindly provided by Masa H. Sato (Kyoto), SEC3A-GFP lines [25] were kindly provided by Tijs Ketelaar (Wageningen), the GFP-ARPC2A line [23] was kindly provided by Kateřina Schwarzerová (Prague), and the PI(4,5)P_2-reporter line (P15Y) [29] was kindly provided by Yvon Jaillais (Lyon). To generate transgenic Col-0 lines expressing GFP-tagged FER, Col-0 was transformed with pFER::FER-GFP containing pMDC111 [64], kindly provided by Ueli Grossniklaus (Zurich).

Information on all genes referenced in this work, including mutant alleles and sources is provided in Supplementary Information, **Table S1**.

RNA extraction and expression analysis

Seedlings were grown on mesh on a ¼ MS plate. Root tissue was harvested 10 dag, immediately frozen in liquid nitrogen and ground in a tissue lyser (Qiagen) with metal beads. Total RNA was extracted using the RNeasy Plant Mini Kit (Qiagen). After DNAse digest (Thermo Fischer Scientific), 0.5 µg total RNA was used for cDNA synthesis with oligo(dT) primers (RevertAid First Strand cDNA Synthesis Kit, Thermo Fischer Schientific). To test for the presence of Gef3 mRNA, 2µl of this cDNA was used for PCR amplification (40 cycles). The primers used for the expression analysis are listed in Supplementary Information, **Table S2**.

Growth conditions and inducible expression

Plants were grown under long day conditions (16 h light) at 21°C. Seedlings used for experiments were grown on ¼ MS medium (pH 5.7) without sucrose, supplied with 0.8% plant agar (Duchefa). Transgenic plants transformed with an estradiol inducible construct were induced with ¼ MS medium containing 20 µM Estradiol (Stock 20 mM in Ethanol) and 0.01% Silwet L77. The time after induction differed between the individual expression constructs and ranged from 3 – 12 h to get sufficient signal for imaging. In general, for imaging of protein localization using inducible expression constructs, time after induction was as low as possible to avoid overexpression artefacts.

310 **Plant transformation and selection**

311 The agrobacterium strain GV3101::pMP90RK pre-transformed with the helper plasmid pSoup was
312 used for all transformations of *Arabidopsis thaliana*. Plants were transformed using floral dipping
313 and transgenic T1 plants were recovered after the appropriate selection. Selection of constructs
314 containing mTurquoise2 (mTrq2) was done on plates containing 50 µg/ml Kanamycin. T1 Selection
315 of constructs containing mCitrine (mCit) was done on soil spraying 3x within 2 weeks (7 – 21 day
316 old seedlings) with Basta®-Solution containing 200 µg/ml Glufosinate-ammonium and 0.05%
317 Tween20. Further generations were selected on plates containing Basta®-Solution to a
318 concentration of 7.5 µg/ml Glufosinate-ammonium. At least 10 independent transgenic lines per
319 expression construct were recovered and checked for fluorescence. The used lines were selected
320 upon good fluorescence and least phenotype and confirmed by PCR.
321

322 **Molecular cloning**

323 All cloning for expression vectors used in Arabidopsis was performed using the GreenGate system
324 [65] and base vector pGGZ003 was used for all expression constructs. A List of all expression
325 constructs including module composition and tagging site is provided in Supplementary
326 Information, **Table S3**. Where internal BsaI (Eco31I) sites were present, they were mutated fusing
327 two PCR fragments, with one mutating the internal BsaI site by an altered primer sequence at this
328 site. After cloning the individual modules into the entry vectors, the complete fragment was checked
329 by sequencing. To confirm the correct assembly of modules into pGGZ003, the presence and
330 orientation was checked by sequencing. As fluorophores, mCitrine (mCit) [66] and mTurqoise2
331 (mTrq2) [67] were fused to the gene of interest separated by a short GAGAGA-Linker. mCit was
332 cloned from the Ca^{2+} indicator CerTN-L15, containing the common folding mutations V163A and
333 S175G [68], and made monomeric by introducing the A206K mutation. mTrq2 was cloned from the
334 Addgene vector LifeAct-mTrq2 (ID #36201). A List of all primers used for molecular cloning is
335 provided in Supplementary Information, **Table S2**.
336 For estradiol inducible expression constructs [69], the XVE gene was fused to the promoter (635
337 bp) and terminator of *UBI10* (AT4G05320). This expression cassette was cloned in reverse
338 orientation into the entry vector pGGA000 together with the oLexA minimal 35S promoter element.
339 Both elements were separated by a 560 bp spacer. This resulted in a single module that could be
340 used as a promoter module for GreenGate cloning.
341 For expression of genes under control of their native promoter, the following sequences upstream
342 of the start codon were cloned into pGGA000: *GEF3* -1743 bp; *GEF4* -1500 bp; *GEF10* -1534 bp;
343 *GEF11* -1458 bp; *GEF12* -701 bp; *ROP2* -1503 bp; *PIP5K3* -1193 bp.
344 For the mbSUS and rBiFC analysis, constructs (listed in Supplementary Information, **Table S3**)
345 were generated using Gateway technology or the 2in1 cloning system (Grefen and Blatt 2012).
346 Coding sequences were PCR-amplified and inserted via 'BP' recombination into either pDONR207,
347 pDONR221-P1P4, or pDONR221-P3P2, respectively, and confirmed by sequencing. Resulting

348 'Entry constructs' were cloned via 'LR' recombination into Destination vectors for either mbSUS or
349 rBiFC [70].
350

351 **Phenotyping of knockout and overexpression mutant lines**

352 Primary roots (7 dag) were used for all phenotyping experiments. For phenotyping of knockout
353 mutant lines the distance of the first bulge to the root tip was defined. The first visible swelling of
354 the cell outline was defined as first bulge, even when this morphological change was very little. The
355 root hair density was analyzed in the next 2 mm. The root hair length was analyzed measuring root
356 hairs growing perpendicular to the root in a region 3-6 mm away from the root tip. For phenotyping
357 the overexpression lines, roots were induced by spraying with medium containing 20 µM Estradiol.
358 The position of the root tip was marked just after induction and normal growing roots were imaged
359 and analyzed 24-26 hours after induction (h.a.i.). A region approximately 2-4 mm from the root tip
360 was used for the analysis of the overexpression phenotype.
361

362 **Propidium iodide staining**

363 Primary roots (7dag) were stained for 5 min in 10 ug/ml propidium iodide (diluted in 1/4MS, from
364 1mg/ml Stock), washed in medium and imaged directly. The staining of different root tissues is very
365 uneven. For better visualization of brighter and dimmer regions the gamma of the images was
366 adjusted (See image processing).
367

368 **Ratiometric Bimolecular Fluorescence analyses (rBiFC)**

369 *Agrobacterium*-mediated transient transformation of 4-6 week old *N. benthamiana* leaves with 2in1
370 rBiFC constructs as described previously [71]. Fluorescence intensities were recorded 36h post
371 infiltration for approximately 30 images per construct as described in [49]. Ratios between
372 complemented YFP fluorescence and RFP were calculated and plotted using BoxplotR.
373 Immunoblotting verified protein expression utilizing anti-MYC conjugated to peroxidase antibodies
374 and anti-HA peroxidase conjugated antibodies, respectively.
375

376 **Mating-based Split Ubiquitin Assay ('Cyto-SUS')**

377 Bait/Cub fusion and preys/Nub fusions were generated by cloning the coding region for *GEF3* and
378 different *ROP2* versions into the Gateway-compatible vectors pMetOYC-Dest and pNX35-Dest,
379 respectively. These were transformed into haploid yeast strains THY.AP4 (Cub fusion) and
380 THY.AP5 (Nub fusions) as described previously [72]. After mating, diploid yeasts were dropped in
381 10 times OD dilutions on vector- (CSM-Leu-, Trp-, Ura) and interaction-selective media (CSM-Leu-
382 , Trp-, Ura-, Ade-, His-) supplemented with 50 or 500µM methionine. The non-mutated N-terminal
383 ubiquitin moiety (NubI) was used as positive control, and NubI13G (empty vector) as negative

control [70]. Protein expression was verified in haploid yeast using antibodies against the VP16 domain for the Cub fusion or the HA epitope tag for the Nub fusions.

Microfluidic device (RootChip-8S) fabrication and on-chip plant cultivation

Microfluidic device fabrication and on-chip plant cultivation were performed as described in [46]. Briefly, Arabidopsis seedlings were grown in pipette tips filled with solidified medium and interfaced with poly(dimethylsiloxane) (PDMS) RootChip-8S devices 4-5 days after germination under sterile conditions. Media perfusion through the microfluidic channels was controlled precisely using a peristaltic pump (DNE GmbH; volumetric flow rate in each channel, 5 µl/min).

Bright-field and fluorescence imaging

Live-cell fluorescence imaging was performed on a custom-built spinning-disk confocal microscope, consisting of a Nikon Ti-E stand, equipped with 20x multi-immersion (N.A. 0.75) and 60x water immersion (N.A. 1.2) objectives (Nikon), a motorized stage (Applied Scientific Instrumentation, USA), a spinning disk with customized hole pattern (CREST Optics, Italy), a motorized filter wheel (Cairn Research, UK), a laser launch (Omicron, Germany), and an EMCCD camera (Photometrics, USA). Image acquisition was operated through Nikon NIS Elements software or Micro-Manager [73]. mCitrine-labeled proteins were excited using a laser emitting at the wavelength of 515 nm; mTrq2-labeled proteins were excited at 440 nm. Bandpass filter specifications were 542nm/20 for mCit emission and 480nm/40 for mTrq2. Chlorophyll autofluorescence was recorded using 561 nm excitation and emission filter specifications of 630nm/92. Root hair phenotyping was performed by transmitted light microscopy on a Nikon SMZ18 stereo microscope, equipped with SHR Plan Apo 0.5x (N.A. 0.075) and 2x (N.A. 0.3) objectives (Nikon) and an Orca Flash 4.0 sCMOS camera (Hamamatsu, Japan). Imaging of the propidium iodide stained root tips expressing different *GEF*::mCit-*GEF* fusions was performed on a Leica SP5 point scanning confocal microscope with a 20x water immersion objective (N.A 0.7), using 1x Zoom, Pinhole 1AU, 1024x1024 pixel scanning field, 400 Hz scanning speed, 2x line average and 2µm Z-Steps as settings. mCit was excited with the 514 nm line of an Argon-Laser and emission light was collected between 520-550 nm. Propidium iodide was exited with a 561 nm laser and emission light was collected between 570-650 nm. Both channels were imaged in sequential scans to avoid crosstalk using Hybrid-Detectors (Gain 200).

Image Processing, data analysis and software

All image processing, image analysis and measurements was done using FIJI (ImageJ) [74], further data analysis was done in Microsoft Excel, if not mentioned otherwise. As statistical test, t-tests (two-tailed, unequal variances) were performed in Excel. A gaussian filter (radius 0.8) and a rolling ball (radius 100) background subtraction was applied to all shown images. The “Royal” lookup table

was used for images shown in intensity pseudo color. Kymographs were generated using the multi-kymograph plugin in FIJI. For images of propidium iodide (PI) staining for visualization of the root outlines, the gamma settings were adjusted to 0.75 to reduce the contrast between weakly and strongly stained regions of the root. The adjustment was only done in the PI channel. The signal of the mCitrine-fusions was not altered.

Polarity indices were analyzed on the original unprocessed images by measuring in 3 by 15 pixel regions at the RHID, outside the RHID and outside the root, as a background value. This background value was subtracted from both regions and the value outside the RHID was divided by the RHID value. This polarity index was calculated for each cell within a root hair file, all files were aligned to the first cell with a visible bulge and the average polarity index for each developmental step was calculated. A signal was defined as polar, if its value differed (p-value <0.05, according to two-tailed t-test with unequal variances) to the polarity index of the membrane marker GFP-Lti6b.

Box plots were created using BoxPlotR (http://shiny.chemgrid.org/boxplotr/), an R-based web-tool provided by the Tyers (Montreal) and Rappsilber (Edinburgh) labs. For all plots number of measurements (n) is given. Center lines show the medians; box limits indicate the 25th and 75th percentiles as determined by R software; whiskers extend 1.5 times the interquartile range from the 25th and 75th percentiles, outliers are represented by dots; crosses represent sample means; bars indicate 95% confidence intervals of the means. For each box plot shown, the value of significance (*p*) according to two tailed Student's t-test are indicated.

ACKNOWLEDGMENTS

We are grateful to Dominique Bergmann (Stanford), Sheila McCormick (UC Berkeley) for detailed comments on our manuscript. We thank Karin Schumacher (U. Heidelberg) and Thomas Dresselhaus (U. Regensburg) for helpful advice, all members of the Grossmann lab and our colleagues at COS Heidelberg for inspiring discussions and their active support. We thank Jan Lohmann (Heidelberg), Markus Grebe (Potsdam), Masa Sato (Kyoto), Tijs Ketelaar (Wageningen), Kateřina Schwarzerová (Prague), Yvon Jaillais (Lyon), and Ueli Grossniklaus (Zurich) for sharing materials and Karin Schumacher and Thomas Holstein (both Heidelberg) for access to microscopes. This work was supported by a grant from the Deutsche Forschungsgemeinschaft (GR 4559/3-1), research group funds from the excellence cluster CellNetworks to G.G., seed funding through the SFB1101, an Emmy Noether fellowship (GR 4251/1-1) to C.G., a PhD-student grant from the Carl-Zeiss-Stiftung to D.G.M., and financial support by ETH Zürich to C.E.S.

AUTHOR CONTRIBUTIONS

The study was conceived by P.D. and G.G.; P.D., A.R., V.A.F.S., D.G.M., L.Y.A., and N.F.K. performed experiments; P.D., A.R., V.A.F.S., D.G.M., L.Y.A., C.G. and G.G. analyzed data. C.E.S. and G.G. designed the microfluidic device. J.F.E. designed the spinning disk microscope and gave advice about the imaging procedure. P.D., A.R. and G.G. prepared figures and wrote the manuscript with input from all coauthors. All authors read and approved the final version of the manuscript.

REFERENCES

[1] Riquelme M. Tip growth in filamentous fungi: a road trip to the apex. Annu Rev Microbiol 2013;67:587–609. doi:10.1146/annurev-micro-092412-155652.

[2] Rounds CM, Bezanilla M. Growth Mechanisms in Tip-Growing Plant Cells. Annu Rev Plant Biol 2013. doi:10.1146/annurev-arplant-050312-120150.

[3] Russell SA, Bashaw GJ. Axon guidance pathways and the control of gene expression. 2017. doi:10.1002/dvdy.24609.

[4] Molendijk AJ, Bischoff F, Rajendrakumar CS, Friml J, Braun M, Gilroy S, et al. Arabidopsis thaliana Rop GTPases are localized to tips of root hairs and control polar growth. Embo J 2001;20:2779–88. doi:10.1093/emboj/20.11.2779.

[5] Jones MA, Shen J-J, Fu Y, Li H, Yang Z, Grierson CS. The Arabidopsis Rop2 GTPase is a positive regulator of both root hair initiation and tip growth. Plant Cell 2002;14:763–76. doi:10.1105/tpc.010359.

[6] Bi E, Park H-O. Cell polarization and cytokinesis in budding yeast. Genetics 2012;191:347–87. doi:10.1534/genetics.111.132886.

[7] Ikeda Y, Men S, Fischer U, Stepanova AN, Alonso JM, Ljung K, et al. Local auxin biosynthesis modulates gradient-directed planar polarity in Arabidopsis. Nat Cell Biol 2009;11:731–8. doi:10.1038/ncb1879.

[8] Fischer U, Ikeda Y, Ljung K, Serralbo O, Singh M, Heidstra R, et al. Vectorial information for Arabidopsis planar polarity is mediated by combined AUX1, EIN2, and GNOM activity. Curr Biol 2006;16:2143–9. doi:10.1016/j.cub.2006.08.091.

[9] Kiefer CS, Claes AR, Nzayisenga J-C, Pietra S, Stanislas T, Hüser A, et al. Arabidopsis AIP1-2 restricted by WER-mediated patterning modulates planar polarity. Development 2015;142:151–61. doi:10.1242/dev.111013.

[10] Fu Y, Li H, Yang Z. The ROP2 GTPase controls the formation of cortical fine F-actin and the early phase of directional cell expansion during Arabidopsis organogenesis. Plant Cell 2002;14:777–94.

[11] Carol RJ, Takeda S, Linstead P, Durrant MC, Kakesova H, Derbyshire P, et al. A RhoGDP dissociation inhibitor spatially regulates growth in root hair cells. Nature 2005;438:1013–6. doi:10.1038/nature04198.

[12] Chang F, Gu Y, Ma H, Yang Z. AtPRK2 Promotes ROP1 Activation via RopGEFs in the Control of Polarized Pollen Tube Growth. Mol Plant 2013;6:1187–201. doi:10.1093/mp/sss103.

[13] Hwang J-U, Gu Y, Lee Y-J, Yang Z. Oscillatory ROP GTPase activation leads the oscillatory polarized growth of pollen tubes. Mol Biol Cell 2005;16:5385–99. doi:10.1091/mbc.E05-05-0409.

[14] Hwang J-U, Vernoud V, Szumlanski A, Nielsen E, Yang Z. A tip-localized RhoGAP controls cell polarity by globally inhibiting Rho GTPase at the cell apex. Curr Biol 2008;18:1907–16. doi:10.1016/j.cub.2008.11.057.

[15] Lin Y, Wang Y, Zhu JK, Yang Z. Localization of a Rho GTPase Implies a Role in Tip Growth and Movement of the Generative Cell in Pollen Tubes. Plant Cell 1996;8:293–303. doi:10.1105/tpc.8.2.293.

[16] Yalovsky S, Bloch D, Sorek N, Kost B. Regulation of Membrane Trafficking, Cytoskeleton Dynamics, and Cell Polarity by ROP/RAC GTPases. Plant Physiol 2008;147:1527–43. doi:10.1104/pp.108.122150.

[17] Zhang Y, McCormick S. A distinct mechanism regulating a pollen-specific guanine nucleotide exchange factor for the small GTPase Rop in Arabidopsis thaliana. Proc Natl Acad Sci USA 2007;104:18830–5. doi:10.1073/pnas.0705874104.

[18] Kost B, Lemichez E, Spielhofer P, Hong Y, Tolias K, Carpenter C, et al. Rac homologues and compartmentalized phosphatidylinositol 4, 5-bisphosphate act in a common pathway to regulate polar pollen tube growth. J Cell Biol 1999;145:317–30. doi:10.1083/jcb.145.2.317.

[19] Cutler SR, Ehrhardt DW, Griffitts JS, Somerville CR. Random GFP::cDNA fusions enable visualization of subcellular structures in cells of Arabidopsis at a high frequency. Proc Natl Acad Sci USA 2000;97:3718–23.

[20] Kusano H, Testerink C, Vermeer JEM, Tsuge T, Shimada H, Oka A, et al. The Arabidopsis Phosphatidylinositol Phosphate 5-Kinase PIP5K3 is a key regulator of root hair tip growth. Plant Cell 2008;20:367–80. doi:10.1105/tpc.107.056119.

[21] Foreman J, Demidchik V, Bothwell JH, Mylona P, Miedema H, Torres MA, et al. Reactive oxygen species produced by NADPH oxidase regulate plant cell growth. Nature 2003;422:442–6. doi:10.1038/nature01485.

[22] Takeda S, Gapper C, Kaya H, Bell E, Kuchitsu K, Dolan L. Local positive feedback regulation determines cell shape in root hair cells. Science 2008;319:1241–4. doi:10.1126/science.1152505.

[23] Havelková L, Nanda G, Martinek J, Bellinvia E, Sikorová L, Šlajcherová K, et al. Arp2/3 complex subunit ARPC2 binds to microtubules. Plant Science 2015;241:96–108. doi:10.1016/j.plantsci.2015.10.001.

[24] Ichikawa M, Hirano T, Enami K, Fuselier T, Kato N, Kwon C, et al. Syntaxin of Plant Proteins SYP123 and SYP132 Mediate Root Hair Tip Growth in Arabidopsis thaliana. Plant Cell Physiol 2014;55:790–800. doi:10.1093/pcp/pcu048.

[25] Zhang Y, Immink R, Liu C-M, Emons A-M, Ketelaar T. The Arabidopsis exocyst subunit SEC3A is essential for embryo development and accumulates in transient puncta at the plasma membrane. New Phytol 2013;199:74–88. doi:10.1111/nph.12236.

[26] Xing S, Mehlhorn DG, Wallmeroth N, Asseck LY, Kar R, Voss A, et al. Loss of GET pathway orthologs in Arabidopsis thaliana causes root hair growth defects and affects SNARE abundance. Proc Natl Acad Sci USA 2017;114:E1544–53. doi:10.1073/pnas.1619525114.

[27] Zhao Y, Araki S, Wu J, Teramoto T, Chang Y-F, Nakano M, et al. An expanded palette of genetically encoded Ca^{2+} indicators. Science 2011;333:1888–91. doi:10.1126/science.1208592.

[28] Keinath NF, Waadt R, Brugman R, Schroeder JI, Grossmann G, Schumacher K, et al. Live Cell Imaging with R-GECO1 Sheds Light on flg22- and Chitin-Induced Transient $[Ca^{2+}]_{cyt}$ Patterns in Arabidopsis. Mol Plant 2015;8:1188–200. doi:10.1016/j.molp.2015.05.006.

[29] Simon MLA, Platre MP, Assil S, van Wijk R, Chen WY, Chory J, et al. A multi-colour/multi-affinity marker set to visualize phosphoinositide dynamics in Arabidopsis. Plant J 2014;77:322–37. doi:10.1111/tpj.12358.

[30] Duan Q, Kita D, Li C, Cheung AY, Wu H-M. FERONIA receptor-like kinase regulates RHO GTPase signaling of root hair development. Proc Natl Acad Sci USA 2010;107:17821–6. doi:10.1073/pnas.1005366107.

[31] Lin D, Nagawa S, Chen J, Cao L, Chen X, Xu T, et al. A ROP GTPase-dependent auxin signaling pathway regulates the subcellular distribution of PIN2 in Arabidopsis roots. Curr Biol 2012;22:1319–25. doi:10.1016/j.cub.2012.05.019.

[32] Jeon BW, Hwang JU, Hwang Y, Song WY, Fu Y, Gu Y, et al. The Arabidopsis Small G Protein ROP2 Is Activated by Light in Guard Cells and Inhibits Light-Induced Stomatal Opening. Plant Cell 2008;20:75–87. doi:10.1105/tpc.107.054544.

[33] Xu T, Wen M, Nagawa S, Fu Y, Chen J-G, Wu M-J, et al. Cell surface- and rho GTPase-based auxin signaling controls cellular interdigitation in Arabidopsis. Cell 2010;143:99–110. doi:10.1016/j.cell.2010.09.003.

[34] Fu Y, Gu Y, Zheng Z, Wasteneys G, Yang Z. Arabidopsis interdigitating cell growth requires two antagonistic pathways with opposing action on cell morphogenesis. Cell 2005;120:687–700. doi:10.1016/j.cell.2004.12.026.

[35] Li H, Lin Y, Heath RM, Zhu MX, Yang Z. Control of pollen tube tip growth by a Rop GTPase-dependent pathway that leads to tip-localized calcium influx. Plant Cell 1999;11:1731–42.

[36] Bourne HR, Sanders DA, McCormick F. The GTPase superfamily: a conserved switch for diverse cell functions. Nature 1990;348:125–32. doi:10.1038/348125a0.

[37] Hodge RG, Ridley AJ. Regulating Rho GTPases and their regulators. Nat Rev Mol Cell Biol 2016;17:496–510. doi:10.1038/nrm.2016.67.

[38] Schmidt A, Lv Z, Großhans J. ELMO and Sponge specify subapical restriction of Canoe and formation of the subapical domain in early Drosophila embryos. Development 2018;145:dev157909. doi:10.1242/dev.157909.

[39] Birnbaum K, Shasha DE, Wang JY, Jung JW, Lambert GM, Galbraith DW, et al. A gene expression map of the Arabidopsis root. Science 2003;302:1956–60. doi:10.1126/science.1090022.

[40] Brady SM, Orlando DA, Lee J-Y, Wang JY, Koch J, Dinneny JR, et al. A high-resolution root spatiotemporal map reveals dominant expression patterns. Science 2007;318:801–6. doi:10.1126/science.1146265.

[41] Borges F, Gomes G, Gardner R, Moreno N, McCormick S, Feijó JA, et al. Comparative Transcriptomics of Arabidopsis Sperm Cells. Plant Physiol 2008;148:1168–81. doi:10.1104/pp.108.125229.

[42] Berken A, Thomas C, Wittinghofer A. A new family of RhoGEFs activates the Rop molecular switch in plants. Nature 2005;436:1176–80. doi:10.1038/nature03883.

[43] Qiu J-L, Jilk R, Marks MD, Szymanski DB. The Arabidopsis SPIKE1 Gene Is Required for Normal Cell Shape Control and Tissue Development. Plant Cell 2002;14:101–18. doi:10.1105/tpc.010346.

[44] Grossmann G, Guo W-J, Ehrhardt DW, Frommer WB, Sit RV, Quake SR, et al. The RootChip: an integrated microfluidic chip for plant science. Plant Cell 2011;23:4234–40. doi:10.1105/tpc.111.092577.

[45] Jones AM, Danielson JÅ, Manojkumar SN, Lanquar V, Grossmann G, Frommer WB. Abscisic acid dynamics in roots detected with genetically encoded FRET sensors. eLife 2014;3:e01741. doi:10.7554/eLife.01741.

[46] Stanley CE, Shrivastava J, Brugman R, Heinzelmann E, van Swaay D, Grossmann G. Dual-flow-RootChip reveals local adaptations of roots towards environmental asymmetry at the physiological and genetic levels. New Phytol 2018;217:1357–69. doi:10.1111/nph.14887.

[47] Kang E, Zheng M, Zhang Y, Yuan M, Yalovsky S, Zhu L, et al. The Microtubule-Associated Protein MAP18 Affects ROP2 GTPase Activity during Root Hair Growth. Plant Physiol 2017;174:202–22. doi:10.1104/pp.16.01243.

[48] Li H, Shen JJ, Zheng ZL, Lin Y, Yang Z. The Rop GTPase switch controls multiple developmental processes in Arabidopsis. Plant Physiol 2001;126:670–84.

[49] Grefen C, Blatt M. A 2in1 cloning system enables ratiometric bimolecular fluorescence complementation (rBiFC). Biotechniques 2012;53. doi:10.2144/000113941.

[50] Grefen C, Obrdlik P, Harter K. The Determination of Protein-protein Interactions by the Mating-based Split-ubiquitin system (mbSUS). Methods Mol Biol 2008;479:1–17. doi:10.1007/978-1-59745-289-2_14.

[51] Huang GQ, Li E, Ge F-R, Li S, Wang Q, Zhang CQ, et al. Arabidopsis RopGEF4 and RopGEF10 are important for FERONIA-mediated developmental but not environmental regulation of root hair growth. New Phytol 2013;200:1089–101. doi:10.1111/nph.12432.

614 [52] Payne RJH, Grierson CS. A theoretical model for ROP localisation by auxin in
615 Arabidopsis root hair cells. PLoS ONE 2009;4:e8337. doi:10.1371/journal.pone.0008337.

616 [53] Bonello TT, Perez-Vale KZ, Sumigray KD, Peifer M. Rap1 acts via multiple mechanisms
617 to position Canoe and adherens junctions and mediate apical-basal polarity
618 establishment. Development 2018;145:dev157941. doi:10.1242/dev.157941.

619 [54] Peterson J, Zheng Y, Bender L, Myers A, Cerione R, Bender A. Interactions between the
620 bud emergence proteins Bem1p and Bem2p and Rho-type GTPases in yeast. J Cell Biol
621 1994;127:1395–406. doi:10.1083/jcb.127.5.1395.

622 [55] Nern A, Arkowitz RA. A GTP-exchange factor required for cell orientation. Nature
623 1998;391:195–8. doi:10.1038/34458.

624 [56] Zheng Y, Bender A, Cerione RA. Interactions among proteins involved in bud-site
625 selection and bud-site assembly in Saccharomyces cerevisiae. J Biol Chem
626 1995;270:626–30. doi:10.1074/jbc.270.2.626.

627 [57] Roemer T, Madden K, Chang J, Snyder M. Selection of axial growth sites in yeast
628 requires Axl2p, a novel plasma membrane glycoprotein. Genes & Development
629 1996;10:777–93. doi:10.1101/gad.10.7.777.

630 [58] Chant J, Corrado K, Pringle JR, Herskowitz I. Yeast BUD5, encoding a putative GDP-
631 GTP exchange factor, is necessary for bud site selection and interacts with bud
632 formation gene BEM1. Cell 1991;65:1213–24.

633 [59] Bender A, Pringle JR. Multicopy suppression of the cdc24 budding defect in yeast by
634 CDC42 and three newly identified genes including the ras-related gene RSR1. Proc Natl
635 Acad Sci USA 1989;86:9976–80. doi:10.1073/pnas.1714058114.

636 [60] Chiou J-G, Balasubramanian MK, Lew DJ. Cell Polarity in Yeast. Annu Rev Cell Dev Biol
637 2017;33:annurev–cellbio–100616–060856. doi:10.1146/annurev-cellbio-100616-060856.

638 [61] Wedlich-Soldner R, Wai SC, Schmidt T, Li R. Robust cell polarity is a dynamic state
639 established by coupling transport and GTPase signaling. J Cell Biol 2004;166:889–900.
640 doi:10.1083/jcb.200405061.

641 [62] Yamaguchi Y, Ota K, Ito T. A Novel Cdc42-interacting Domain of the Yeast Polarity
642 Establishment Protein Bem1 IMPLICATIONS FOR MODULATION OF MATING
643 PHEROMONE SIGNALING. J Biol Chem 2007;282:29–38.
644 doi:10.1074/jbc.M609308200.

645 [63] Butty AC, Pryciak PM, Huang LS, Herskowitz I, Peter M. The role of Far1p in linking the
646 heterotrimeric G protein to polarity establishment proteins during yeast mating. Science
647 1998;282:1511–6.

648 [64] Escobar-Restrepo J-M, Huck N, Kessler S, Gagliardini V, Gheyselinck J, Yang W-C, et
649 al. The FERONIA receptor-like kinase mediates male-female interactions during pollen
650 tube reception. Science 2007;317:656–60. doi:10.1126/science.1143562.

651 [65] Lampropoulos A, Sutikovic Z, Wenzl C, Maegele I, Lohmann JU, Forner J. GreenGate---
652 a novel, versatile, and efficient cloning system for plant transgenesis. PLoS ONE
653 2013;8:e83043. doi:10.1371/journal.pone.0083043.

654 [66] Griesbeck O, Griesbeck O, Baird GS, Baird GS, Campbell RE, Campbell RE, et al.
655 Reducing the Environmental Sensitivity of Yellow Fluorescent Protein. J Biol Chem
656 2001;276:29188–94. doi:10.1074/jbc.M102815200.

657 [67] Goedhart J, Stetten von D, Noirclerc-Savoye M, Lelimousin M, Joosen L, Hink MA, et al.
658 Structure-guided evolution of cyan fluorescent proteins towards a quantum yield of 93%.
659 Nat Commun 2012;3:509. doi:10.1038/ncomms1738.

660 [68] Heim N, Garaschuk O, Friedrich MW, Mank M, Milos RI, Kovalchuk Y, et al. Improved
661 calcium imaging in transgenic mice expressing a troponin C–based biosensor. Nat Meth
662 2007;4:127–9. doi:10.1038/nmeth1009.

663 [69] Zuo J, Niu Q-W, Chua N-H. An estrogen receptor-based transactivator XVE mediates

highly inducible gene expression in transgenic plants. Plant J 2000;24:265–73. doi:10.1046/j.1365-313x.2000.00868.x.

[70] Xing S, Wallmeroth N, Berendzen KW, Grefen C. Techniques for the Analysis of Protein-Protein Interactions in Vivo. Plant Physiol 2016;171:727–58. doi:10.1104/pp.16.00470.

[71] Mehlhorn DG, Wallmeroth N, Berendzen KW, Grefen C. 2in1 Vectors Improve In Planta BiFC and FRET Analyses. The Plant Endoplasmic Reticulum, vol. 1691, New York, NY: Humana Press, New York, NY; 2018, pp. 139–58. doi:10.1007/978-1-4939-7389-7_11.

[72] Asseck LY, Wallmeroth N, Grefen C. ER Membrane Protein Interactions Using the Split-Ubiquitin System (SUS). The Plant Endoplasmic Reticulum, vol. 1691, New York, NY: Humana Press, New York, NY; 2018, pp. 191–203. doi:10.1007/978-1-4939-7389-7_15.

[73] Edelstein A, Amodaj N, Hoover K, Vale R, Stuurman N. Computer control of microscopes using μManager. Curr Protoc Mol Biol 2010;Chapter 14:Unit14.20. doi:10.1002/0471142727.mb1420s92.

[74] Schindelin J, Arganda-Carreras I, Frise E, Kaynig V, Longair M, Pietzsch T, et al. Fiji: an open-source platform for biological-image analysis. Nat Meth 2012;9:676–82. doi:10.1038/nmeth.2019.

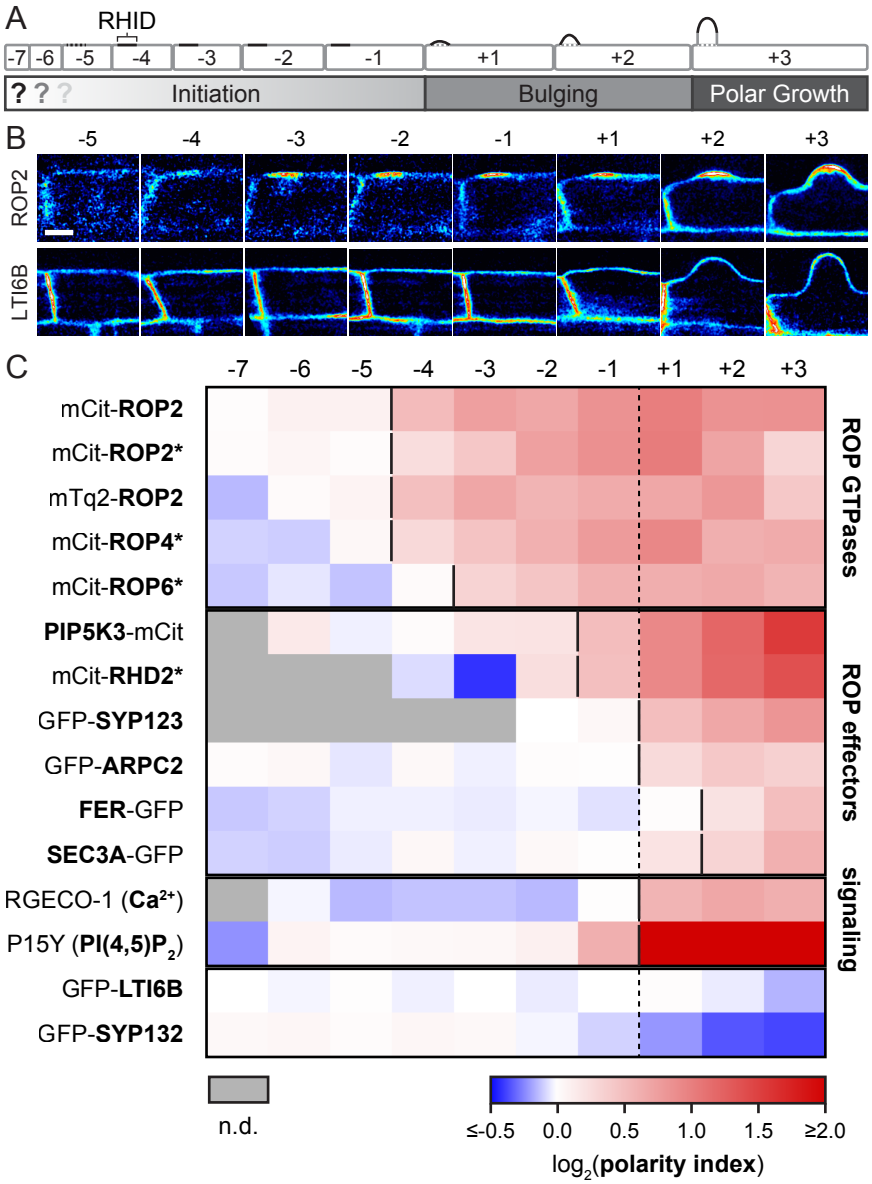

Figure 1. Timeline analysis of protein accumulation at the RHID.

(**A**) Model of root hair development in an epidermal cell file. During the initiation phase the root hair initiation domain (RHID) emerges in elongating trichoblasts and the tip growth machinery is assembled using an unknown mechanism. Stages -1/+1 mark the bulge out at the RHID followed by the transition into polar growth. (**B**) Comparison of mCit-ROP2 and GFP-LTI6B protein localization at the RHID in different stages of root hair development. Scale bar, 10 µm. (**C**) Protein accumulation at the RHID throughout the early development of root hairs in 13 different marker lines. Genes are sorted by the timing of accumulation within their group of protein function. Color coding represents the polarity index (signal intensity in/out of RHID; $\log_2$ scale) for each developmental step. (n.d.: no data). For each stage average polarity index values from multiple cells are shown (see **Supplemental figure 1** for details). Stages -7 to -1 represent cells in the initiation phase before bulging, +1 to +3 cells after bulging. The homogeneously distributed membrane protein Lti6b is used as reference for protein accumulation. Listed genes were fused to either eGFP, mTurquoise2 (mTq2) or mCitrine (mCit), under control of their own promoters, except for UBQ10::P15Y ($PI(4,5)P_2$ reporter), 35S::LTI6B and genes under control of an estradiol inducible promoter (indicated by an asterisk).

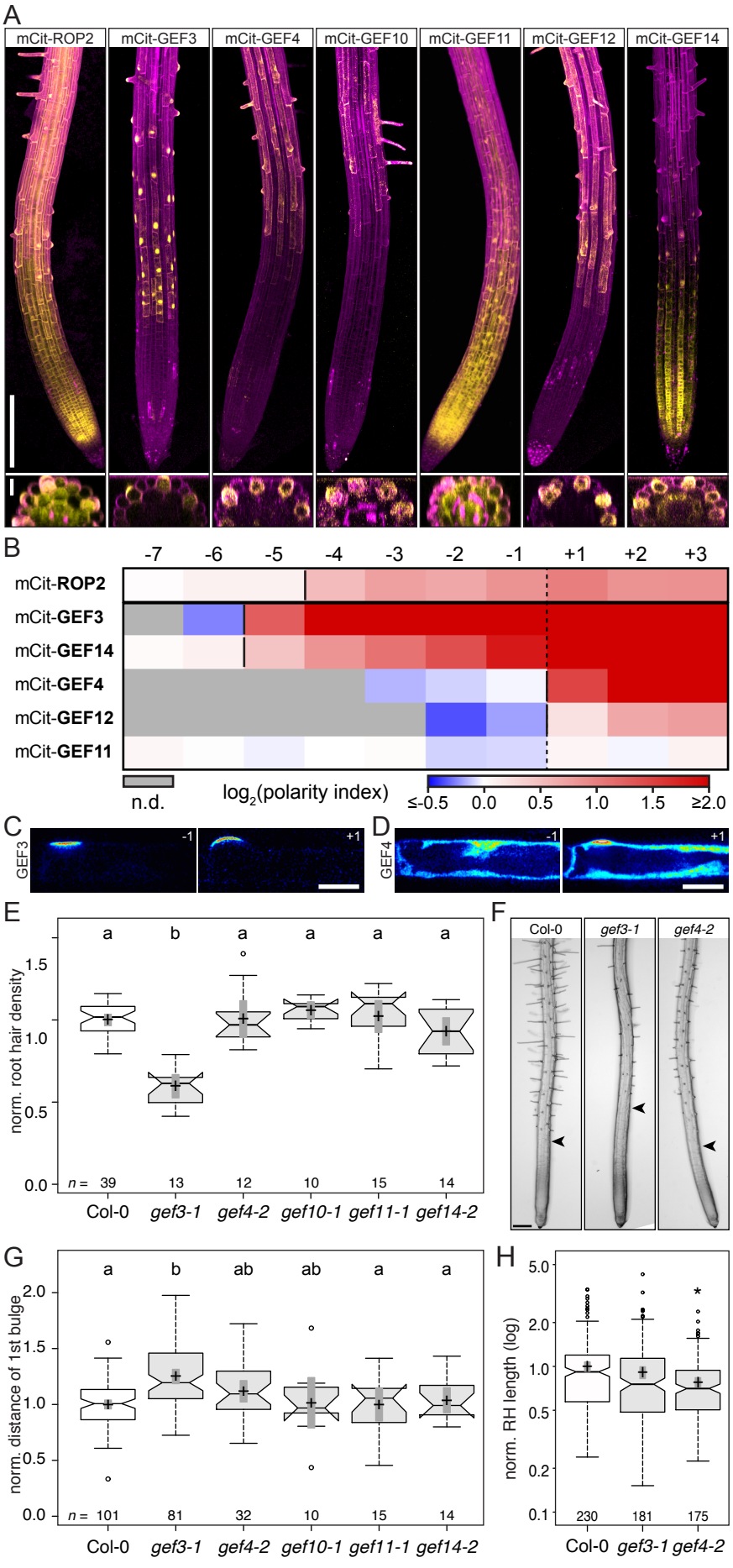

Figure 2. Functional analysis of ROPGEFs in the root epidermis identifies GEF3 to be required for efficient root hair emergence.

(**A**) Roots expressing mCit fusion proteins (yellow) under their respective promoters. To visualize root and cell outlines, roots were stained with propidium iodide (magenta). Top panel: Maximum intensity projection of the root tip. Scale bar, 200 µm. lower Panel: Optical cross section through the root in the elongation zone to visualize the tissues expressing the respective constructs. Scale bar, 20 µm. (**B**) Timeline analysis of protein accumulation at the RHID for selected GEFs in comparison to ROP2. GEFs are sorted by timing of accumulation at the RHID. Polarity index measurement and calculation as in Figure 1. (**C, D**) Subcellular localization (intensity-coded representation) of mCit-GEF3 and mCit-GEF4 in cells just before (-1) and after bulging (+1). Scale bars, 20µm. (**E, G**) Quantification of root hair density (**E**) and distance (**G**) of first bulge to the root tip for selected GEFs, normalized to Col-0. Letters show results of an ANOVA-Test (significance value 0.01), with same letters indicating no significant differences. (**F**) Representative root tips of WT (Col-0), gef3-1 and gef4-2 mutant lines. Arrowheads indicate the first bulge. (H) Quantification of hair length 3-6 mm away from root tip in gef3-1 and gef4-2 mutant lines compared to Col-0. Normalized values are shown in log2 scale to account for the high variability in individual hairs. Asterisk indicates $p \leq 0.05$ according to two-tailed students t-test. Values in (**E, G, H**) were normalized to corresponding Col-0 values for each independent experiment.

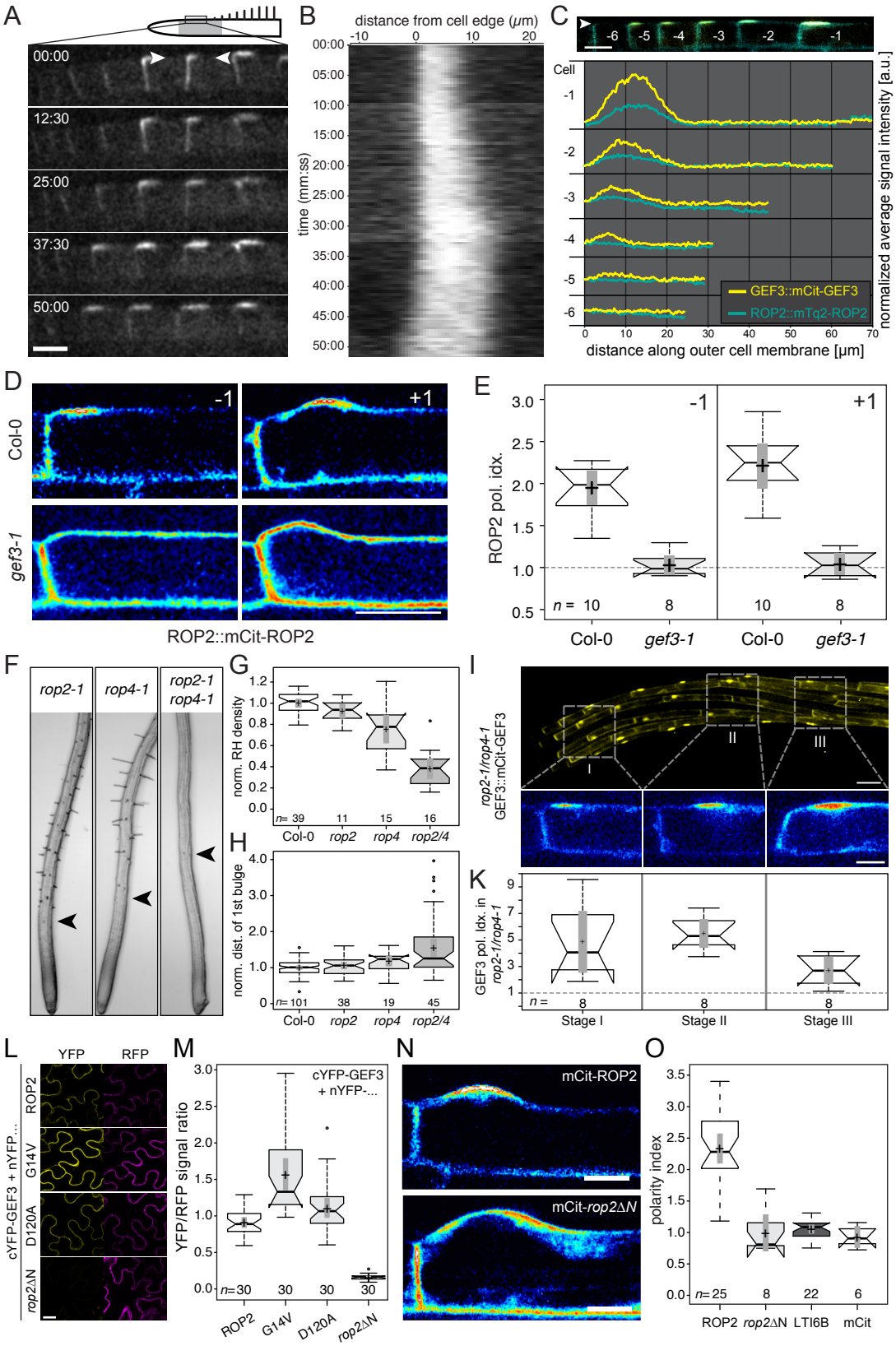

Figure 3. GEF3 is necessary for polar ROP2 recruitment during root hair initiation.

(**A**) Time-lapse imaging of GEF3::mCit-GEF3 in the RootChip-8S. A root hair cell file in the early elongation zone is shown. Multiple stages of protein accumulation can be seen in each still image. The time series was registered to compensate cell movement due to root growth. Numbers indicate time (mm:ss). Scale bar, 20µm. (**B**) The kymograph was generated along the outer cell flank (left-right orientation) between arrow heads in (**A**). The vertical axis depicts time; the horizontal axis depicts distance. Note the gradual expansion of the emerging mCit-GEF3 domain over time until approximately 30 min and a stable domain size after that. (**C**) Colocalization and intensity profiles of GEF3 and ROP2 along RH cell files. Top: exemplary root hair cell file expressing ROP2::mTq2-ROP2 (cyan) and GEF3::mCit-GEF3 (yellow). Cells are labeled from youngest cells (-6) to oldest cell (-1) before bulging. Bottom: average intensity profiles of mTrq2-ROP2 (grey) and mCit-GEF3 (black) along the outer cell periphery (line width 3 px) of 6 root hair cell files (arrowhead indicates direction of line measurement). (**D**) Subcellular localization and (**E**) quantification of mCit-ROP2 polarity at the RHID in Col-0 and the *gef3-1* mutant in root hair cells just before (-1) and after bulging (+1). Scale bar, 20µm. (**F**) Representative root tips of *rop2-1, rop4-1* and *rop2-1xrop4-1* mutant lines. Arrowheads indicate the first bulge. (**G, H**) Quantification of root hair density and distance of first bulge to the root tip, normalized to Col-0 (as reference, the data for Col-0 in Figure 3 are reused). Values are normalized to corresponding Col-0 values for each independent experiment. (**I**) GEF3::mCit-GEF3 expression and localization in *rop2-1xrop4-1* mutant background. Upper panel: overview of the elongation zone. Lower panel: subcellular localization of mCit-GEF3 in cells of the early (I), middle (II), and late (III) elongation zone. (**K**) Quantification of the polarity index of GEF3::mCit-GEF3 in *rop2-1xrop4-1* mutant background. Stages are chosen as indicated in (**I**). (**L**) Representative images of an rBiFC assay in tobacco epidermal cells for each combination tested. All images were recorded using identical conditions and settings, correction for brightness and contrast during image processing was kept equal except for the exemplary YFP image of *rop2*ΔN, which was set brighter to visualize the very low background signal. (**M**) Quantification of ratiometric BiFC experiments. YFP signals were normalized to the corresponding RFP signal to allow comparison of interaction strength. (N) Confocal image of root hair cells expressing estradiol inducible mCit-ROP2 or mCit-*rop2*∆N. Scale bar, 10µm. (**O**) Quantification of polarity index of the constructs shown in (**N**) and compared to the non-polar membrane marker GFP-LTI6B and free mCitrine.

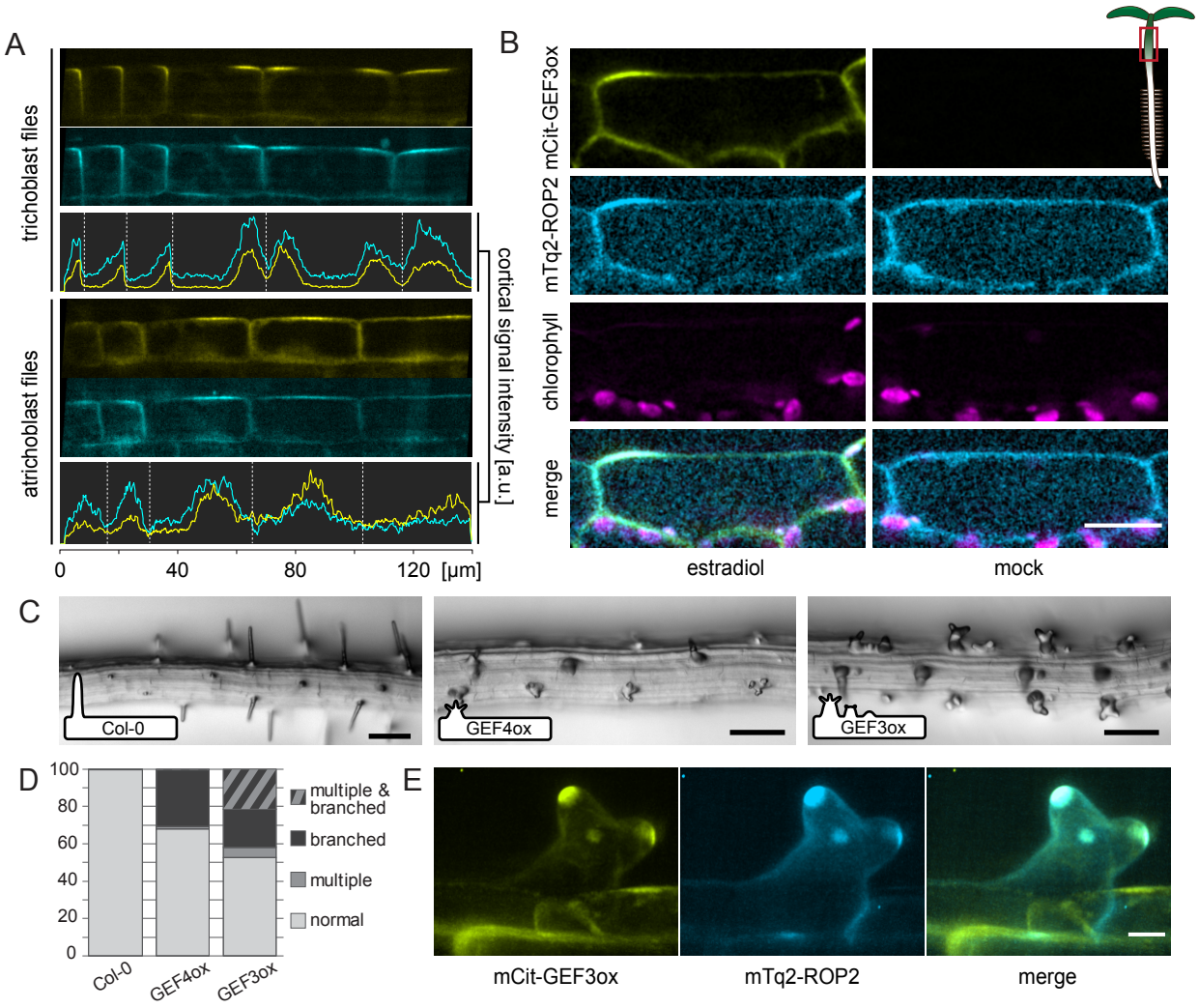

Figure 4. GEF3 initiates the formation of polar growth domains.

(**A**) Localization of ROP2::mTq2-ROP2 (cyan) in roots overexpressing mCit-GEF3 (yellow). Top: representative cell files of trichoblasts and atrichoblasts, both show ectopic accumulations of both markers. Bottom: intensity profiles along cell periphery of cells shown on the left. Dashed lines indicate cell borders. (**B**) Subcellular localization of ROP2::mTq2-ROP2 (cyan) in hypocotyl cells ectopically expressing mCit-GEF3 (yellow). Chlorophyll autofluorescence is shown in magenta. Scale bar, 20 µm. (**C**) Representative images of Col-0 (upper) and roots overexpressing mCit-GEF4 (middle) and mCit-GEF3 (lower) (24h after estradiol induction). Inserts show an idealized sketch of the predominant root hair shape. Scale bars, 100 µm. (**D**) Frequency of phenotypes (induction of multiple hairs, bulges with multiple tips, and combined phenotypes) induced by overexpression of lines shown in (**C**) in % of total observed hairs (n(Col-0)=337; n(mCit-GEF3ox)=238; n(mCit-GEF4ox)=233). (**E**) Colocalization of mCit-GEF3 (yellow) and ROP2::mTq2-ROP2 (cyan) in branched root hairs, 24 hours after estradiol induction of mCit-GEF3 overexpression. Scale bar, 20 µm.